

2003

Monte Carlo Analysis of GaN-Based Gunn Oscillators for Microwave Power Generation

R. P. Joshi

Old Dominion University

V. Sridhara

Old Dominion University

P. Shah

R. D. del Rosario

Follow this and additional works at: https://digitalcommons.odu.edu/ece_fac_pubs



Part of the [Physics Commons](#)

Repository Citation

Joshi, R. P.; Sridhara, V.; Shah, P.; and del Rosario, R. D., "Monte Carlo Analysis of GaN-Based Gunn Oscillators for Microwave Power Generation" (2003). *Electrical & Computer Engineering Faculty Publications*. 156.

https://digitalcommons.odu.edu/ece_fac_pubs/156

Original Publication Citation

Joshi, R. P., Sridhara, V., Shah, P., & Rosario, R. D. d. (2003). Monte Carlo analysis of GaN-based Gunn oscillators for microwave power generation. *Journal of Applied Physics*, 93(8), 4836-4842. doi:10.1063/1.1562734

Monte Carlo analysis of GaN-based Gunn oscillators for microwave power generation

R. P. Joshi^{a)} and V. Sridhara

Department of Electrical and Computer Engineering, Old Dominion University, Norfolk, Virginia 23529-0246

P. Shah and R. D. del Rosario

U.S. Army Research Laboratory, Adelphi, Maryland 20783

(Received 12 December 2002; accepted 29 January 2003; corrected 23 December 2011)

Monte Carlo studies of transferred electron oscillators based on bulk wurtzite GaN are presented. Two structures have been examined: (i) devices with the conventional single notch structure, and (ii) repetitive structures with serial segments to fashion a “multiple domain” device. Wurtzite material has been chosen because of the higher drift velocity and because analytical expressions for the band structure have recently become available. Performance parameters of interest such as the operating frequency, output power, and conversion efficiency are calculated. Variations due to changes in temperature, biasing voltage, and device length are also included. It is shown that multidomain Gunn diodes can lead to significant improvements in output power over conventional, single-transit structure, and so such multiple GaN diodes merit serious experimental study. © 2003 American Institute of Physics. [DOI: 10.1063/1.1562734]

I. INTRODUCTION

Over the past five years or so, the nitride material system has been the focus of intense research.^{1–8} Advantages of these direct, large-band-gap materials include the ability to sustain large electric field ($\sim 10^8$ V m⁻¹, which bodes well for device downscaling and higher breakdown voltage), high saturation velocities ($\sim 1.5 \times 10^5$ m s⁻¹), lower generation noise, radiation hardness, and high-temperature operation. GaN-based electronic amplifiers are projected to have significant improvement over silicon devices.⁹ The nitrides have also shown promise as emitters and detectors,^{10–12} Bragg reflectors,¹³ light-emitting diodes (LEDs),¹⁴ sensors for jet and automobile engines,¹⁵ and space-based operation in the solar blind region (~ 260 – 290 nm).

The high-field drift velocity of bulk GaN is larger than that of GaAs^{16,17} due to the higher intervalley separation and the larger optical phonon energy. GaN lends itself to heterostructure fabrication, and the presence of a strong internal polarization can create very high sheet carrier densities ($> 10^{17}$ m⁻²). Experimental demonstrations of large radio-frequency (rf) power densities, as measured in watts per millimeter of the gate periphery, have already been made.^{18–21} The higher thermal conductivity of GaN relative to GaAs and use of SiC substrates^{22,23} should help alleviate the thermal management issue. These aspects collectively enhance the prospects of GaN for microwave power amplification particularly at the X band and higher frequencies.^{24–26}

Since the satellite valley effective electronic masses of both zinc-blende and wurtzite-phase GaN are higher than in the lowest conduction bands, the material appears to show promise as a large-signal oscillator based on the transferred

electron effect.²⁷ The presence of an inflection point in the Γ_1 -valley band structure of the zinc-blende phase has also been suggested as a source of negative differential resistance (NDR).²⁸ As compared to the traditional GaAs and InP-based negative differential resistance (NDR) devices,^{29,30} the conversion efficiency and power handling capacity should be superior. Despite the potential, there have not been many studies on this subject to the best of our knowledge. The only reports appear to be by Alekseev and Pavlidis²⁷ for wurtzite GaN based on transient hydrodynamic simulations, and by Zhao *et al.*³¹ for the zinc-blende phase. A full Monte Carlo treatment of the time-dependent transferred electron problem is more accurate and desirable than the hydrodynamic scheme. Previous studies have often used the steady-state velocity-field characteristics^{16,32} and relied on somewhat older band structure data. For example, previous reports were based on Γ_1 - Γ_2 and M - L intervalley separations of 1.9 and 2.1 eV, respectively.^{33,34} More recent calculations³⁵ suggest a Γ_1 , M - L , Γ_3 , L_1 , A_1 ordering, with the two lowest valleys 2.2717 and 2.4 eV above Γ_1 . In view of this, it is perhaps important to reexamine the large-signal response characteristics of GaN-based oscillators based on recent data.

Here we provide Monte Carlo based studies of oscillatory behavior in wurtzite GaN. Two device structures have been examined: (i) devices with the conventional single notch structure, and (ii) repetitive structures with serial segments, each consisting of the basic notch element to fashion a “multiple domain” device. Wurtzite material has been chosen because analytical expressions of parameters, such as the nonparabolicity coefficient and effective masses are now available³⁵ to facilitate an accurate Monte Carlo analysis. In addition, the larger drift velocities predicted for the wurtzite material at high fields bodes well for promoting higher frequencies for Gunn diode operation. Performance parameters

^{a)}Electronic mail: rjoshi@odu.edu

TABLE I. Parameters used in the Monte Carlo calculations for wurtzite GaN.

Parameter	Value
Lattice constants in meter (a, c)	$3.189 \times 10^{-10}, 5.185 \times 10^{-10}$
Dielectric constants $k(0), k(\infty)$	9.5, 5.35
Density (g cm^{-3})	6.095
Acoustic velocity (m s^{-1})	4.33×10^5
Effective mass m_{\parallel} (T_1, U and T_3 valley)	0.1846, 0.3858, 3.6227
Effective mass m_{\perp} (T_1, U and T_3 valley)	0.2283, 3.03, 0.2856
Valley separation (eV)	0.0, 2.2717, 2.4
Nonparabolicity factors T_1 (eV^{-1})	0.37
Nonparabolicity factors U valley (eV^{-1})	$3.03(m_{\perp})$ and $0.385(m_{\parallel})$
Nonparabolicity factors T_3 valley (eV^{-1})	$0.22(m_{\perp})$ and $4.455(m_{\parallel})$
Longitudinal optical phonon energy (eV)	0.092
Intervalley phonon energy (eV)	0.065
Acoustic deformation potential (eV)	8.0
Zero-order equivalent intervalley deformation potential (eV/cm)	0.5×10^9
Zero-order nonequivalent intervalley deformation potential (eV/cm)	1.0×10^9
First-order intervalley potential (eV)	5.0

of interest such as the operating frequency and conversion efficiency are calculated. Variations due to changes in temperature, biasing voltage, and device length are also included. The repetitive structure is studied since, to the best of our knowledge, the potential utility of multiple domain structures (MDS) has not been examined in the context of GaN Gunn diodes. The use of multiple domain diodes was first suggested by Thim³⁶ and Robrock³⁷ and experimentally verified by Slater and Harrison.³⁸ The primary advantage of using a multiple-domain structure is that the operating frequency can be increased for a fixed total device length since the basic repetitive segment then scales down with domain number N . Alternatively, by serially cascading the basic Gunn diode unit structure, the total length can be increased without adversely affecting the operating frequency. However, to maintain impedance matching, the device area scales up by N , thereby increasing the current. Since the applied voltages have to be scaled up by N (to maintain the internal field), an N^2 enhancement in the output power can potentially result. Efficiency enhancements, with such N^2 scaling, have been predicted for GaAs Gunn diodes.³⁹ Here, we provide a quantitative evaluation for multidomain wurtzite GaN diodes using the Monte Carlo simulation approach.

II. MONTE CARLO SIMULATION DETAILS

Details of the Monte Carlo implementation have been discussed elsewhere with simulation results shown to match published data for bulk GaN rather well.⁴⁰ A three-valley Monte Carlo model had been used that included electron interactions with acoustic modes via the deformation potential, polar optical phonon interactions, and zero- and first order intervalley deformation potential scattering.⁴¹ A 65 meV phonon was assumed to adequately represent deformation potential scattering, and a 92 meV phonon value was used for the polar optical process. Besides, ionized impurity based on the Brooks–Herring approach and intervalley deformation potential processes were also considered. The piezoelectric scattering was excluded, since it has been shown to be negligible at temperatures of 300 K and beyond. Non-equivalent intervalley scattering events were taken into ac-

count amongst all three valley types, governed by a single deformation potential and phonon energy. Screening was incorporated with the random phase approximation in the long wavelength limit. The value of the inverse screening length β was obtained as $\beta(t) = [n e^2 / \epsilon k_B T_e(t)]^{0.5}$ where n is the electron density, e the electronic charge, k_B the Boltzmann constant, and T_e the effective electron temperature. This effective temperature was evaluated at each time step of the Monte Carlo simulation with the following equation:¹⁶

$$T_e(t) = [2/(3k_B)] \sum_I f_I \{0.5 m_I \langle v^2 \rangle_I - 0.5 m_I v_{dI}^2\}. \quad (1)$$

In the above, f_I , m_I , $\langle v^2 \rangle_I$, and v_{dI}^2 refer to the electron fraction, effective mass, mean-square velocity, and drift velocity, respectively, for the i th valley and the index I runs over the three valleys. The T_e represents an *ad hoc* parameter¹⁶ and is not a real electron temperature. Degeneracy and Pauli exclusion was included based on a rejection technique implementation first proposed by Lugli and Ferry.⁴²

The material parameters required for the bulk GaN simulations were generally taken from the published literature,^{17,32,43} and are given in Table I. For wurtzite-phase GaN, the minimum is located at the Γ_1 point, and a three-dimensional view of the Brillouin zone including points within the irreducible wedge is shown in Fig. 1. The effective masses have been calculated to be 0.2283 and 0.1846

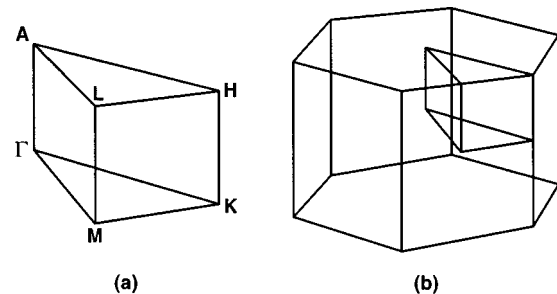


FIG. 1 (a) Brillouin zone schematic including the various symmetry points within the irreducible wedge. (b) View of the full Brillouin zone including the irreducible wedge.

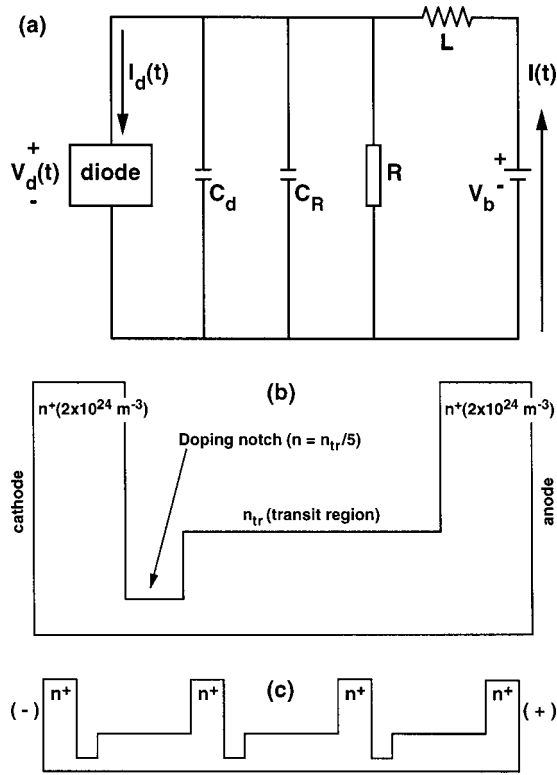


FIG. 2. Schematic pertaining to the device simulations. (a) Lumped electrical circuit, (b) doping profile of the conventional GaN notch diode, and (c) schematic of a three transit region multiple GaN Gunn diode.

along the perpendicular and parallel directions, respectively, with a nonparabolicity coefficient of about 0.37 eV^{-1} . The satellite valleys are at the U point that is two-thirds of the way between the L - and M - symmetry points, with an energy separation of 2.2717 eV . According to the calculations by Goano *et al.*,³⁵ the next highest valley is located at the Γ_3 point, 2.4 eV above Γ_3 . Finally, the valleys at the L_1 and A_1 points are located 2.5 and 2.6 eV , respectively, above the conduction band minima. The effective masses for the M - L minima are anisotropic. As given in Table I the mass is 3.0375 (along Γ - A_1), 0.3158 (along K - H), and 0.3858 (along the M and L points). The corresponding nonparabolicity coefficient also depend on the direction, and are reported to be: -1.0325 eV^{-1} (along Γ - A_1), 0.2164 eV^{-1} (along K - H), -0.174 eV^{-1} (along M), and 0.9686 eV^{-1} (along L). Such anisotropic features were included in the present Monte Carlo approach. For the Γ_3 valley, the effective masses along the parallel and perpendicular directions were taken to be 3.6227 and 0.2856 , respectively. The nonparabolicity factors are given to be 4.4554 parallel to the c axis and 0.22 along the perpendicular directions.

For a more realistic simulation of the microwave oscillator, the GaN device was embedded in a parallel resonant circuit as shown in Fig. 2(a). This allows for the inclusion of circuit effects, permits performance evaluation at the fundamental frequency and other harmonics, and the assessment of circuit parameter variations. Time-varying voltage boundary conditions were applied to the GaN structure, and the device currents computed based on the Monte Carlo particle flows. The total current was obtained by solving the related Kirch-

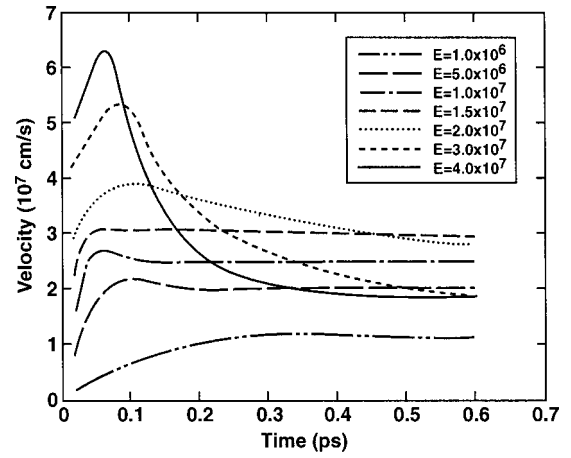


FIG. 3. Monte Carlo results of the transient electron drift velocity at 300 K in wurtzite GaN for different electric fields

hoff equations. The displacement current can be accounted for by using the cold capacitance procedure.⁴⁴ In our simulations, the device structure was taken to have a cross-sectional area of 10^{-9} m^2 . The doping profile for the conventional notch-type device is shown in Fig. 2(b). The two heavily doped end regions with densities of $2 \times 10^{24} \text{ m}^{-3}$ serve as the n^+ contacts. The doping level “ n ” of the transit region was taken to vary within the $5 \times 10^{22} - 2 \times 10^{23} \text{ m}^{-3}$ range. Thus the doping level of the drift region was chosen to be much larger than typically used for GaAs or InP Gunn devices.^{45,46} Since the mobility of GaN is lower in comparison to both GaAs and InP, the time required to build up a stable domain is higher for the same background doping. The higher doping chosen here helps offset the lower mobility value. The notch at the cathode end is required to create the local nonuniformity that helps launch the accumulation or dipole-domain mode instabilities. The equilibrium density of the notch was set at 20% of the transit region. The dead-zone lies in this region. Figure 2(c) shows the schematic of a repetitive Gunn diode structure with three transit regions. Such structures with multiple zones were also used in the present simulations. For the electrical circuit, a 20Ω resistor, an external capacitance of 0.05 pF , and 0.12 nH inductor were assumed.

III. RESULTS AND DISCUSSION

Results of the Monte Carlo simulation for bulk wurtzite GaN at 300 K are given and discussed first. The primary objective was to test the current GaN model predictions against more sophisticated calculations that have included a full band structure. A 10 000-electron Monte Carlo code was used with a 2 fs time step. Figure 3 shows the transient drift velocity of the electronic ensemble in bulk GaN at 300 K for different values of the electric field parameter. An upper-bound of 300 kV/cm was chosen to prevent the electronic energies from becoming excessively large. This precaution was necessary, since the present simulation does not include a full band structure, but instead relies on a simple nonparabolic approach to the energy bands. The steady-state, 300 K, velocity-field characteristics obtained from the results of Fig.

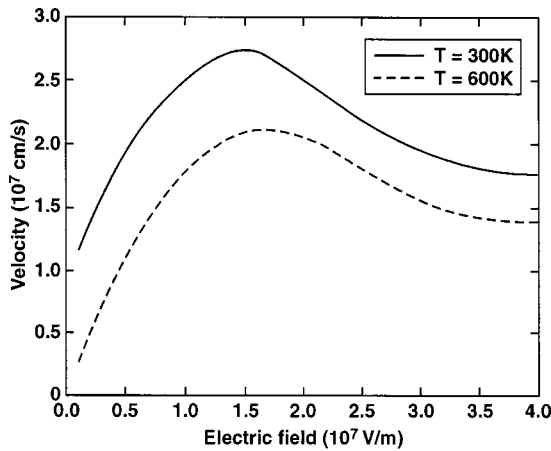


FIG. 4. Monte Carlo results of the steady-state, velocity-field characteristics for electrons at temperatures of 300 and 600 K.

3 at long times are given in Fig. 4. Also shown are results at 600 K. A peak velocity in excess of $2 \times 10^5 \text{ ms}^{-1}$ is predicted for the 600 K temperature. This value is far larger than that for GaAs at room temperature, and underscores the utility of GaN for high temperature (or high power) operation. The 300 K results facilitate a direct comparison with previous reports that took account of a full band-structure calculation.³² The threshold field for the negative differential conductance for the 300 K case is predicted to be around 180 kV/cm. This value and the overall velocity-field curve are in good agreement with the report by Kolnich *et al.*³² A peak steady state drift velocity of about $2.7 \times 10^5 \text{ ms}^{-1}$ is predicted for the 300 K case. A gradual decrease in the steady-state drift velocity beyond 180 kV/cm is apparent, but the values remain well over $2 \times 10^5 \text{ ms}^{-1}$ even for electric field as high as 300 kV/cm. With increasing temperature, the velocities reduce due to stronger electron-phonon scattering. Finally, occupancies of the lowest Γ valley as a function of time for the 300 K case are shown in Fig. 5 for various electric fields. Fractional occupancies of 90% and higher are predicted for applied electric field below 160 kV/cm. There is a relatively sharp transition into the satellite valleys for field around 180 kV/cm. Steady-state Γ_1 -valley occupancies

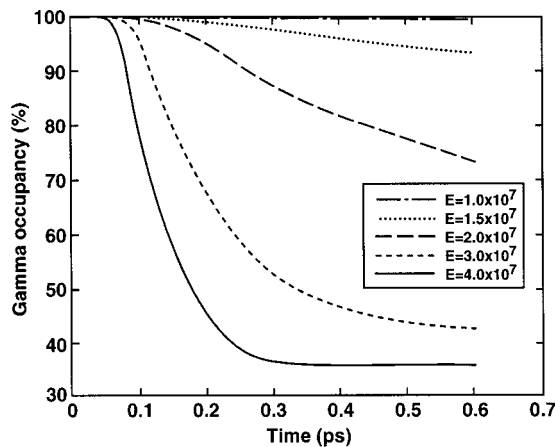


FIG. 5. Simulation results showing the temporal development of the electron populations in the lowest valley at 300 K.

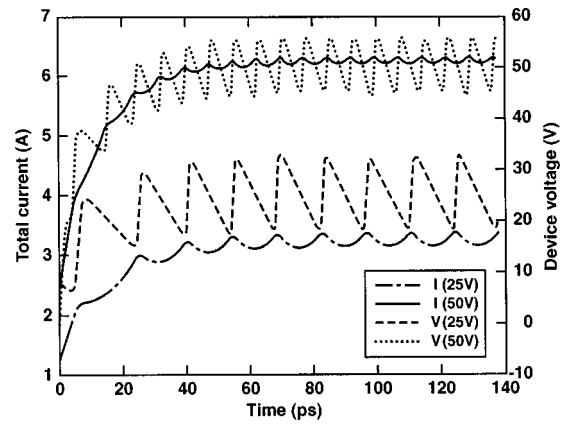


FIG. 6. Simulation results showing the temporal development of the device voltage and total circuit current for a $1.0 \mu\text{m}$ device at 300 K. A 50 V bias was used.

as low as 35% are predicted at our highest field at 300 kV/cm. These results are also fairly close to those obtained by Kolnich *et al.*³² on the basis of a more sophisticated Monte Carlo scheme that included a full band structure. This agreement establishes the validity of the transport parameters used in the present model and underscores its utility as a simple, computational efficient tool for analyzing transport for field below 300 kV/cm.

Having demonstrated the Monte Carlo model, simulations were next carried out for the GaN based Gunn $n^+ - n^- - n - n^+$ notch structure for lengths of the n region around $1.0 \mu\text{m}$ at 300 K. The much smaller length (as compared to the $3.0 \mu\text{m}$ device simulations previously reported²⁷) serves two purposes: (a) Enhanced operating frequency due to lower transit times, and (b) it ensures a higher sinusoidal component at the fundamental mode. Longer devices that operate in dipole domain mode tend to have a flatter response, with a higher nonsinusoidal component since variations in terminal current only take place at the start of every domain formation cycle. The n -doping range of $5 \times 10^{22} - 2 \times 10^{23} \text{ m}^{-3}$ chosen here leads to a ‘ nL ’ product above the $5 \times 10^{16} \text{ m}^{-2}$ threshold³¹ for GaN Gunn oscillations. The circuit of Fig. 2 was incorporated and the initial electron distribution taken to mimic the doping density distribution. The Gunn structure was taken to connect with the tank circuit at $t = 0^+$.

Monte Carlo results at 300 K for the single transit Gunn diode showing the time dependent behavior of the total current and the device voltage are shown in Fig. 6. The device length was taken to be $1.0 \mu\text{m}$, and applied bias was 50 V. The initial transient is simply associated with the commencement of the applied dc bias at time $t = 0$. A steady oscillatory state is reached in about 60 ps, with the operating frequency predicted to be 135 GHz. Results for the simulated frequency dependencies of the generated power and device efficiency were then obtained by running such time dependent simulations for various device voltages, device lengths, and operating temperatures. The results are given in Figs. 7 and 8 for two operating temperatures of 300 and 450 K. At very low biasing levels, the electric field within the GaN device is close to the threshold for NDR, and hence the power output

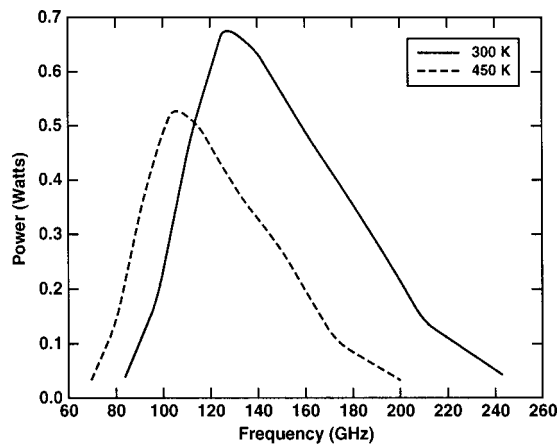


FIG. 7. Monte Carlo results of the power output vs frequency at 300 and 450 K for single domain GaN Gunn diodes.

is low. With increasing bias the output power increases, as does the operating frequency due to the larger average electron velocity. A central maxima thus results, and the general shape is in keeping with previous reports. At very high biasing the transferred electron effect is lost with nearly all carriers residing primarily in the satellite valleys. The curve at the higher temperature of 450 K shifts to lower frequencies due to the reduced carrier velocity and the power output is predicted to drop. Figure 7 shows peak powers to be about 0.665 and 0.525 W at the 300 and 450 K operating temperatures. Since device self-heating effects have not been included here, these values represent an overestimation. In any case, there is considerable improvement over the reported results of about 0.150 W for InP.⁴⁷ This is not surprising, since the threshold field for GaN is roughly ten times larger than in InP. The corresponding efficiencies are shown in Fig. 8 at the 300 and 450 K temperatures. Peak efficiencies of 1.9% and 1.47% are predicted for the single transit region GaN Gunn diode. The room temperature value is higher than that reported for GaAs devices.⁴⁵

Finally, Monte Carlo simulations were performed for GaN diodes with multiple transit segments. The resulting power output as a function of the frequency is given in Fig.

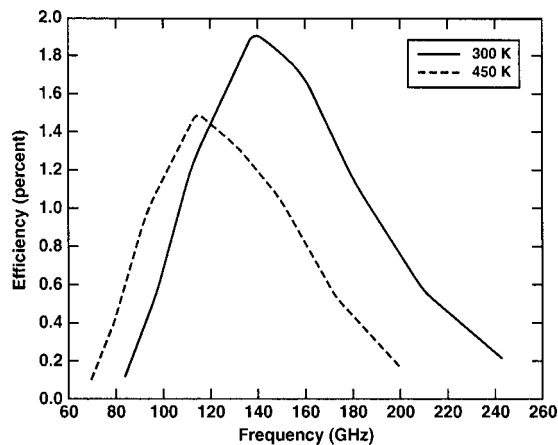


FIG. 8. Simulation results of the device efficiency vs frequency at 300 and 450 K.

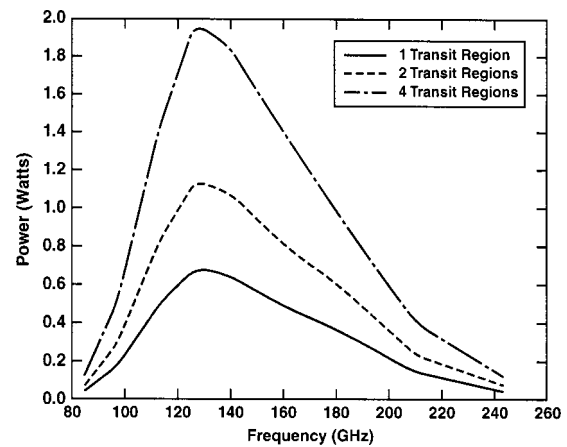


FIG. 9. Results of the power output vs frequency at 300 K for multiple transit segment GaN Gunn diodes. Plots for one, two, and four segments are shown.

9 at 300 K for one, two, and four transit regions. A simplistic expectation is for the output power to scale as N^2 (with N the number of segments) for fixed values of the operating frequency, temperature, and device impedance. This follows from a required scaling in both the voltage (to maintain the device electric field) and device current (due to an increase in area for maintaining the impedance). However, in practice, the benefit of a multiple transit structure might not be quite as significant for a variety of reasons. In a conventional single-transit region device, the injected carriers are all nearly thermalized and have comparable energies. Hence the device noise can be expected to be lower due to a relatively “tightly bunched” carrier distribution, especially for short device lengths. With multiple transit zones, however, the carrier distributions at the start of each successive transit segment might not be completely periodic, nor closely bunched in distribution, and could be nonthermal. Consequently, one can expect a larger variance in the intervalley transfer distance, leading to higher noise. The actual condition at the start of successive domains depends on the thickness and doping of the N^+ layer between the transit regions. Thicker and more strongly doped layers would facilitate better carrier thermalization, but would increase the overall transit time and adversely impact the operating frequency. The absence of a fully thermal distribution at the beginning of each successive transit region also implies that the average carrier energies within the device would tend to be larger. This could lead to enhanced internal power losses because of strong polar-optical phonon scattering, especially within the satellite valleys due to their higher density of states. In addition, with the hot electrons spending a longer fraction of their time within the satellite valleys, the overall speed would be slower, and the swing in the current oscillation reduced. Last, but not least, the higher power losses can be expected to lead to higher internal temperatures and possible thermal gradients due to local hot spots near the successive “virtual anodes.” Both would adversely affect the transport and reduce operating frequency. Collectively then, the useful power output might not scale quite as well as N^2 .

Most of the above issues could be addressed by a three-dimensional Monte Carlo simulation procedure. However, since we have not performed self-consistent electrothermal calculations, the heating aspects and their role in mitigating the Gunn diode response could not be addressed. The thermal analysis as well as the noise characteristics will be presented elsewhere. The Monte Carlo results of the power output versus frequency are given in Fig. 9 at 300 K for one, two, and four transit regions. The device area, however, was not increased for ease of comparison. The results show that the output power does not quite scale as N , but instead is a sublinear function. Hence, by increasing the area, one would not expect the output power enhancement to be quite as large as N^2 . In any case, the power output is certainly better than that of the conventional, single-transit structure, and so the multiple GaN Gunn diode structure does merit serious experimental study.

IV. CONCLUSIONS

The large-signal response characteristics of GaN-based Gunn oscillators were reexamined based on recent band-structure data that has become available for the wurtzite material. Wurtzite GaN is also more interesting since it has been shown to have a higher drift velocity that should promote higher frequencies for Gunn diode operation. Device performance parameters of interest were calculated for two separate situations. First, devices with the conventional single notch structure were simulated to obtain predictions of the output power and conversion efficiency. Then, multiple domain devices containing repetitive serial segments, were analyzed. The repetitive structure has been studied here since, to the best of our knowledge, the benefit and potential of multiple domain structures (MDS) have not been examined in the context of GaN Gunn diodes. Theoretical predictions for GaAs Gunn oscillators call for an N^2 scaling in output power with the number of segments N .

Device parameters such as the operating frequency, power output, and conversion efficiency were obtained. Variations due to changes in temperature, biasing voltage, and device length were also included. As expected, the operating frequency has been shown to fall with increasing temperature due to a lower drift velocity. The results, for a single transit region structure, showed that conversion efficiencies up to about 2% can be attained at 300 K and would be around 1.45% at 450 K. The room temperature value is higher than that reported for GaAs devices. Also, the efficiencies are slightly higher than those calculated elsewhere for GaN on the basis of hydrodynamic models. Corresponding peak power outputs of 0.68 and 0.52 W have been predicted at 300 and 450 K, respectively. Here again, considerable improvement is predicted over other material [e.g., the reported results of about 0.150 W for InP (Ref. 47)]. However, it must be emphasized that since device self-heating effects have not been included here, these values represent an overestimation.

Finally, for multiple-domain structures, considerable improvements in output power have been predicted. Without changing the device area, the output power results were seen

to roughly scale with the number of segments N . Slight deviations (sublinear behavior) seen can be attributed to the loss in absolute repetitiveness from one segment to the next. Hot electron effects and larger average carrier energies contribute to the sublinear behavior. Hence, for devices with scaled increases in area, the output power would not be quite as large as the predicted N^2 factor. Also, the noise for the multidomain devices is expected to be higher than the conventional structures. This factor has not been studied and will be analyzed elsewhere. In any case, the advantage of multiple GaN Gunn diode structures has been made obvious, and such devices do merit serious experimental study.

ACKNOWLEDGMENTS

This work was sponsored in part by a grant from the Army Research Office (No. DAAD19-01-1-0617). Discussions with J. H. Zhao and M. Goano are gratefully acknowledged.

- ¹Y. F. Wu, B. P. Keller, S. Keller, D. Kapolnek, P. Kozodoy, S. P. Denbaars, and U. K. Mishra, *Appl. Phys. Lett.* **69**, 1438 (1996).
- ²S. N. Mohammad, A. Salvador, and H. Morkoc, *Proc. IEEE* **83**, 1306 (1995).
- ³H. Morkoc, *Nitride Semiconductors and Devices* (Springer-Verlag, Heidelberg, 1999).
- ⁴R. P. Joshi, *Appl. Phys. Lett.* **64**, 223 (1994); R. P. Joshi, A. N. Dharamsi, and J. Mcadoo, *ibid.* **64**, 3611 (1994).
- ⁵S. Nakamura, T. Mukai, and M. Senoh, *Appl. Phys. Lett.* **64**, 1687 (1994).
- ⁶R. Gaska, Q. Chen, J. Yang, A. Osinky, M. A. Khan, and M. S. Shur, *IEEE Electron Device Lett.* **18**, 492 (1997).
- ⁷S. Keller, G. Parish, P. T. Fini, S. Heikman, C. H. Chen, N. Zhang, S. P. Denbaars, U. K. Mishra, and Y.-F. Wu, *J. Appl. Phys.* **86**, 5850 (1999).
- ⁸R. Gaska, M. S. Shur, A. D. Bykhovski, A. O. Orlov, and G. L. Snider, *Appl. Phys. Lett.* **74**, 287 (1999).
- ⁹K. Shenai, R. S. Scott, and B. J. Baliga, *IEEE Trans. Electron Devices* **36**, 1811 (1989).
- ¹⁰S. Nakamura, M. Senoh, S. Nagahama, N. Iwasa, T. Yamada, T. Matsushita, H. Kiyoku, Y. Sugimoto, T. Kozaki, H. Umemoto, M. Sano, and K. Chocho, *Jpn. J. Appl. Phys., Part 2* **36**, L1568 (1997).
- ¹¹G. E. Bulman, K. Doverspike, S. T. Sheppard, T. W. Weeks, H. S. Kong, H. M. Dieringer, J. A. Edmond, J. D. Brown, J. T. Swindell, and J. F. Schetzina, *Electron. Lett.* **33**, 1556 (1997).
- ¹²S. Nakamura, M. Senoh, N. Iwasa, S. Nagahama, T. Yamada, and T. Mukai, *Jpn. J. Appl. Phys., Part 2* **34**, L1332 (1995).
- ¹³I. J. Fritz and T. J. Drummond, *Electron. Lett.* **31**, 68 (1995).
- ¹⁴H. Morkoc and S. N. Mohammad, *Wiley Encyclopedia of Electrical and Electronics Engineering*, edited by J. Webster (Wiley, New York, 1999).
- ¹⁵H. Morkoc, *IEEE J. Sel. Top. Quantum Electron.* **4**, 537 (1998).
- ¹⁶U. Bhapkar and M. S. Shur, *J. Appl. Phys.* **82**, 1649 (1997).
- ¹⁷J. D. Albrecht, R. P. Wang, P. P. Ruden, M. Farahmand, and K. F. Brennan, *J. Appl. Phys.* **83**, 4777 (1998).
- ¹⁸W. F. Yu, B. P. Keller, P. Fini, J. Pust, M. Le, N. Nguyen, C. Nguyen, D. Widman, S. Keller, S. P. Denbaars, and U. K. Mishra, *Electron. Lett.* **33**, 1742 (1997).
- ¹⁹S. T. Sheppard, K. Doverspike, W. L. Pribble, S. T. Allen, J. W. Palmour, L. T. Kehias, and T. J. Jenkins, *IEEE Electron Device Lett.* **20**, 161 (1999).
- ²⁰F. Wu, B. P. Keller, S. Keller, D. Kapolnek, S. P. Denbaars, and U. K. Mishra, *IEEE Electron Device Lett.* **17**, 455 (1996).
- ²¹Y. F. Wu, D. Kapolnek, J. P. Ibbetson, P. Parikh, B. P. Keller, and U. K. Mishra, *IEEE Trans. Electron Devices* **48**, 586 (2001).
- ²²D. E. Grider, N. X. Nguyen, and C. Nguyen, *Solid-State Electron.* **43**, 1473 (1999).
- ²³S. Rumyantsev, M. E. Levinshstein, R. Gaska, M. S. Shur, A. Khan, J. W. Yang, G. Simin, A. Ping, and T. Adesida, *Phys. Status Solidi A* **176**, 201 (1999).
- ²⁴G. J. Sullivan, M. Y. Chen, J. A. Higgins, J. W. Yang, Q. Chen, R. L. Pierson, and B. T. McDermott, *IEEE Electron Device Lett.* **19**, 198 (1998).

- ²⁵S. C. Binari, K. Doverspike, G. Kelner, and H. B. Dietrich, *Solid-State Electron.* **41**, 177 (1997).
- ²⁶E. M. Chumbes, J. Smart, T. Prunty, and J. R. Shealy, *IEEE Trans. Electron Devices* **48**, 416 (2001).
- ²⁷E. Alekseev and D. Pavlidis, *Solid-State Electron.* **44**, 941 (2000); E. Alekseev and D. Pavlidis, *Electron. Lett.* **36**, 176 (2000).
- ²⁸S. Krishnamurthy, M. van Schilfgaarde, A. Sher, and A. B. Chen, *Appl. Phys. Lett.* **71**, 1999 (1997).
- ²⁹H. Eisele and G. I. Haddad, *IEEE Microwave Guid. Wave Lett.* **8**, 24 (1998); H. Eisele, A. Rydberg, and G. I. Haddad, *IEEE Trans. Microwave Theory Tech.* **48**, 626 (2000).
- ³⁰P. J. Bulman, G. S. Hobson, and B. C. Taylor, *Transferred Electron Devices* (Academic, New York, 1972).
- ³¹J. H. Zhao, V. Gruzinskis, M. Weiner, M. Pan, P. Shiktorov, and E. Starikov, *Mater. Sci. Forum* **334-342**, 1635 (2000).
- ³²J. Kolnick, I. H. Oguzman, K. F. Brennan, W. Rongping, P. P. Ruden, and W. Yang, *J. Appl. Phys.* **78**, 1033 (1995).
- ³³B. E. Foutz, S. K. O'Leary, M. S. Shur, and L. F. Eastmen, *J. Appl. Phys.* **85**, 7727 (1999).
- ³⁴W. R. L. Lambrecht and B. Segall, in *Properties of Group III Nitrides*, EMIS Datareviews Series, No. 11, edited by J. H. Edgar (Inspec, London, 1994), Chap. 4.
- ³⁵M. Goano, E. Bellotti, E. Ghillino, G. Ghione, and K. F. Brennan, *J. Appl. Phys.* **88**, 6467 (2000).
- ³⁶H. W. Thim, *J. Appl. Phys.* **39**, 3898 (1968).
- ³⁷R. Robrock, *IEEE Trans. Electron Devices* **ED-17**, 93 (1970).
- ³⁸M. Slater and R. I. Harrison, *IEEE Trans. Electron Devices* **ED-23**, 560 (1976).
- ³⁹Y. P. Teoh and G. M. Dunn, *Electron. Lett.* **38**, 830 (2002).
- ⁴⁰T. Li, R. P. Joshi, and C. Fazi, *J. Appl. Phys.* **88**, 829 (2000).
- ⁴¹D. K. Ferry, *Phys. Rev. B* **14**, 1605 (1976).
- ⁴²P. Lugli and D. K. Ferry, *IEEE Trans. Electron Devices* **32**, 2431 (1985).
- ⁴³O. Madelung, *Physics of Group IV Elements and III-V Compounds*, Group III, Vols. 17a and 22a, Landolt-Bornstein New Series (Springer-Verlag, Berlin, 1981).
- ⁴⁴P. A. Blakey and R. K. Froelich, *IEEE Trans. Microwave Theory Tech.* **MTT-31**, 781 (1983).
- ⁴⁵R. Vaidyanathan and R. P. Joshi, *Electron. Lett.* **27**, 1555 (1991).
- ⁴⁶C. Lee and U. Ravaioli, *Electron. Lett.* **26**, 425 (1990).
- ⁴⁷V. Gruzinskis, E. Starikov, P. Shiktorov, L. Reggiani, and L. Varani, *J. Appl. Phys.* **76**, 5260 (1994).